Yokoo, R; Goto, K; Kasahara, J; Athmanathan, V; Braun, J; Paniagua, G; Meyer, TR; Kawasaki, A; Matsuoka, K; Matsuo, A; Funaki, I, Experimental study of internal flow structures in cylindrical rotating detonation engines, PROCEEDINGS OF THE COMBUSTION INSTITUTE, 38, 3, 2021, 3759-3768

Title: **Experimental Study of Internal Flow Structures in Cylindrical Rotating Detonation Engines**

Authors: RYUYA YOKOO[1], KEISUKE GOTO[1], JIRO KASAHARA[1], VENKAT ATHMANATHAN[2], JAMES BRAUN[3], GUILLERMO PANIAGUA[2,3], TERRENCE MEYER[2,3], AKIRA KAWASAKI[1], KEN MATSUOKA[1], AKIKO MATSUO[4], IKKOH FUNAKI[5]

Affiliation 1: Department of Aerospace Engineering, Nagoya University
Furo-cho, Chikusa-ku, Nagoya, Aichi 464-8603, Japan

Affiliation 2: School of Aeronautics and Astronautics, Purdue University,
701 W Stadium Ave, West Lafayette, IN 47907, USA

Affiliation 3: School of Mechanical Engineering, Purdue University,
585 Purdue Mall, West Lafayette, IN 47907, USA

Affiliation 4: Department of Mechanical Engineering, Keio University
3-14-1 Hiyoshi, Kouhoku-ku, Yokohama, Kanagawa 223-8522, Japan

Affiliation 5: Institute of Space and Astronautical Science, Japan Aerospace Exploration Agency
3-1-1 Yoshinodai, Chuo-ku, Sagamihara, Kanagawa 252-5210, Japan

Corresponding author's contact information: JIRO KASAHARA
Department of Aerospace Engineering, Nagoya University
Furo-cho, Chikusa-ku, Nagoya, Aichi 464-8603, Japan
E-mail: kasahara@nuae.nagoya-u.ac.jp
Fax: +81-52-789- 4404

Colloquium: DETONATIONS, EXPLOSIONS, AND SUPERSONIC COMBUSTION

Total Length: 6189 words
(Method: M1)

Main text:	3057 words
Equations:	38 words
Nomenclature:	235 words
References:	384 words
Figures:	2285 words
Tables	190 words

Abstract

The internal flow structures of detonation wave were experimentally analyzed in an optically accessible hollow rotating detonation combustor with multiple chamber lengths. The cylindrical RDC has a glass chamber wall, 20 mm in diameter, which allowed us to capture the combustion self-luminescence. A chamber 70 mm in length was first tested using C_2H_4-O_2 and H_2–O_2 as propellants. Images with a strong self-luminescence region near the bottom were obtained, confirming the small extent of the region where most of the heat release occurs as found in our previous research. Based on the visualization experiments, we tested RDCs with shorter chamber walls of 40 and 20 mm. The detonation wave was also observed in the shorter chambers, and its velocity was not affected by the difference in chamber length. Thrust performance was also maintained compared to the longer chamber, and the short cylindrical RDC had the same specific impulse tendency as the cylindrical (hollow) or annular 70-mm chamber RDC. Finally, we calculated the pressure distributions of various chamber lengths, and found they were also consistent with the measured pressure at the bottom and exit. We concluded that the short-chamber cylindrical RDC with equal length and diameter maintained thrust performance similar to the longer annular RDC, further expanding the potential of compact RDCs.

Keywords

Detonation, Cylindrical Rotating Detonation Engine, Hollow Rotating Detonation Engine, Flow Structure, Optically Accessible Combustor

Nomenclature

A_c	=	cross-sectional area of combustion chamber (= $\pi d_o^2/4$)
D	=	wave velocity of detonation
d	=	diameter
d_o	=	combustion chamber diameter

F = thrust

I_{sp} = specific impulse

$I_{sp,theo}$ = theoretical specific impulse

$I_{sp,\ ie}$ = specific impulse calculated under the assumption of ideally expanded

L = combustion chamber length

$\dot{m}$ = mass flow rate

M = Mach number

p = pressure

p_b = back pressure

p_c = pressure of combustion at chamber bottom

p_{65} = pressure of chamber at z = 65 mm

z = axial position of combustion chamber

z_{rc} = axial position of chemical reaction completion

δ^* = displacement thickness of boundary layer

φ = hole diameter

Φ = equivalence ratio

Subscripts

c = combustion chamber

e = chamber exit

i = initial

ple = plenum

ox = oxidizer

f = fuel

z = axial position

1. Introduction

A detonation wave that is self-sustained and propagates in a premixed fuel-oxidizer mixture has a compression effect ahead of the combustion zone. It therefore features higher combustion product gas temperature and pressure compared to deflagrative combustion [1, 2, 3]. The immediate completion of combustion due to the supersonic combustion wave is also a characteristic of detonation combustion. These advantages encourage the use of detonation combustion in engines, particularly in the aerospace field. Engines based on detonation combustion can lead to a more compact combustor than conventional engines, and may reduce the load on the compressor due to the self-compression effect of detonation combustion [3, 4, 5]. Therefore, various types of combustors using detonative combustion have been proposed. Rotating detonation engines (RDE) and pulse detonation engines (PDE) [6] are the typical forms of such engines; other forms such as a reflective shuttling detonation combustor (RSDC) [7] have also been proposed.

For practical implementation of detonation combustion in engines, the analysis of the internal flow field in detonation engines is crucial. This was addressed by several researchers by means of an optically accessible detonation combustors. Rankin et al. [8] obtained mid-infrared pictures of high-temperature water vapor and ultraviolet images of OH* chemiluminescence in an optically accessible, annular geometry, non-premixed H_2-Air RDC [9]. They described he structure of detonation wave in detail and observed the wave's behavior at various mass flow rates and equivalent ratios. Chacon and Gamba [10] described the detonation sstructure present in an obround geometry combustor and performed 10 Hz OH-PLIF and OH* chemiluminesncec detailed flow field description. They observed non-uniform propagation due to non-ideal conditions of the combustor and "parasitic combustion," which is a deflagration combustion region

accompanying detonation waves [11]. Bohon et al. [12] measured self-luminescence and high-frequency pressure simultaneously in an RDC with various mass flow rates and equivalent conditions, classified the propagation mode of detonation waves by mass flow rate, and suggested that pressure and luminance increase when the wave passes. Athmanathan et al. [13] presented a detailed unsteady dynamic description of the detonation structure through time resolved MHz rate chemiluminescence and complementary URANS simulations. This work revealed the presence of azimuthal reflected shock combustion present in non-premixed annular RDCs. Other researchers have also evaluated thrust performance using methods for conventional rocket engines, such as quasi-one-dimensional (1-D) flow theory [14-15]. Knowlen et al. [14] analyzed the flow field in RDE by Rayleigh flow theory, and found that the exit flow calculated from the conditions downstream and upstream of the detonation wave reached supersonic velocity. Goto et al. [15] evaluated steady performance and heat-load of RDE by utilizing a method designed for conventional rocket engines. These studies describe the presence of complicated flow fields in RDCs and justify detailed time-resolved measurements in optically accessible RDCs.

Typical RDCs have an annular combustor, and generate thrust by a detonation wave rotating at the bottom of a slit chamber. Several studies, however, revealed that RDEs without an inner cylinder also work as a detonation engine [16-20]. Cylindrical, inner-core-less RDEs have potential advantages. Removing the inner cylinder enables a more compact RDE, and solves thermal problems related to the inner cylinder. Tang et al. [16] numerically demonstrated that detonation waves could rotate continuously in a hollow RDE combustion chamber. Wei et al. [17] and Anand et al. [18] also confirmed that it was possible to realize a stable rotating detonation wave experimentally in a cylindrical RDE. Kawasaki et al. [19] and Yokoo et al. [20] investigated the thrust performance of RDE with various inner-cylinder radii, and obtained the critical condition of mass flux. On the other hand, a cylindrical RDE has no channel which sustains the detonation wave, and the wave may tend not to stand perpendicularly to the outer wall. This may weaken the wave and thrust performance, but it

was also confirmed that the performance is the same as an annular design by adjusting the mass flux of the cylindrical RDE. In any case, internal flow structure of the cylindrical RDE has not been analyzed enough whereas the structure of other forms of detonation engines has been as mentioned above.

In this study, we describe the detailed of the detonation structure present in a cylindrical RDC using C_2H_4-O_2 and H_2-O_2 as propellants. Through MHz rate imaging, we observe the combustion zone to originate near the injection site for both ethylene/oxygen and hydrogen/oxygen combinations.. We also compared the self-luminescence observation results to the internal flow numerical model proposed in previous research [20]. In addition to the fuel/oxidizer change, an optimal combustor necessitates a short combustor length. We studied the effects varying the chamber length. The thrust performance and combustion were compared to the experimental results of the cylindrical RDC with a 70-mm long chamber. We found that a cylindrical RDC with a shorter chamber could achieve the same specific impulse as a cylindrical, or even annular, RDC with a longer chamber. We also analyzed the internal flow and revealed that the internal flow model proposed in our previous work could be applied to the various geometrical and supply conditions of the RDC. [20]

2. Experimental apparatus and conditions

Figure 1 presents schematics and Fig. 2 photographs of the rotating detonation combustor (RDC) without an inner core. RDC chambers had 2 types of wall: the stainless steel wall shown in Fig. 1a and Fig. 2a, and the glass wall shown in Fig. 1b and Fig. 2b. Pressure distribution could be measured with the stainless steel wall, and self-luminescence could be observed from the radial direction with the glass wall. Both an acrylic (PMMA) and quartz glass were utilized as the combustor wall of the RDC. Hence, the inside of the chamber during combustion could be observed from the side of the cylinder using a high-speed camera (Shimadzu HPV-X2). The combustion chamber diameter d_o was 20 mm, and the RDC had neither a convergent nor divergent nozzle. The chamber length L of the stainless wall was 70 mm, and L of the glass

wall was varied at 70, 40 and 20 mm. The optically accessible length, however, was $L-12$ mm from the bottom due to the 12-mm long endplate shown in Figs. 1b and 2b.

The RDC had 24-pairs of doublet, impinging injectors on the bottom surface, arranged in circles with diameters of 9 mm for fuel, and 15 mm for oxidizer, as shown in Fig. 1c. The diameter of the injector holes was 0.8 mm, and fuel (from inside) and oxidizer (from outside) impinged at an angle of 45 degrees. A pressure measurement port was also installed at the bottom center. The stainless steel chamber wall and endplate had a pressure measurement port and detonation initiator port, respectively. The RDC was initiated with gunpowder or a pre-detonator. C_2H_4–O_2 and H_2–O_2 were the propellants tested here. In the case of C_2H_4–O_2, we also measured thrust by installing the RDC on the thrust stand, and captured an axial self-luminescence image with a high-speed camera (Phantom, v2011), in addition to the image captured from the side of the RDE with the Shimadzu HPV-X2. For the H_2–O_2 tests, a hydrogen-oxygen pre-detonator charge was fired near the exit to initiate the detonations. The test duration was 300 ms, and the high-speed camera (Shimadzu HPV-X2) was triggered 150 ms after the start of the RDC. Only in Test 7, the camera was also attached to an image intensifier (Lambert Instruments HiCATT, GaAsP enhanced red, 280–800 nm) coupled with a 105-mm UV lens (Nikon, UV-Nikkor) to capture the broadband chemiluminescence, including OH*, blue flame emission and high-temperature water vapor [21].

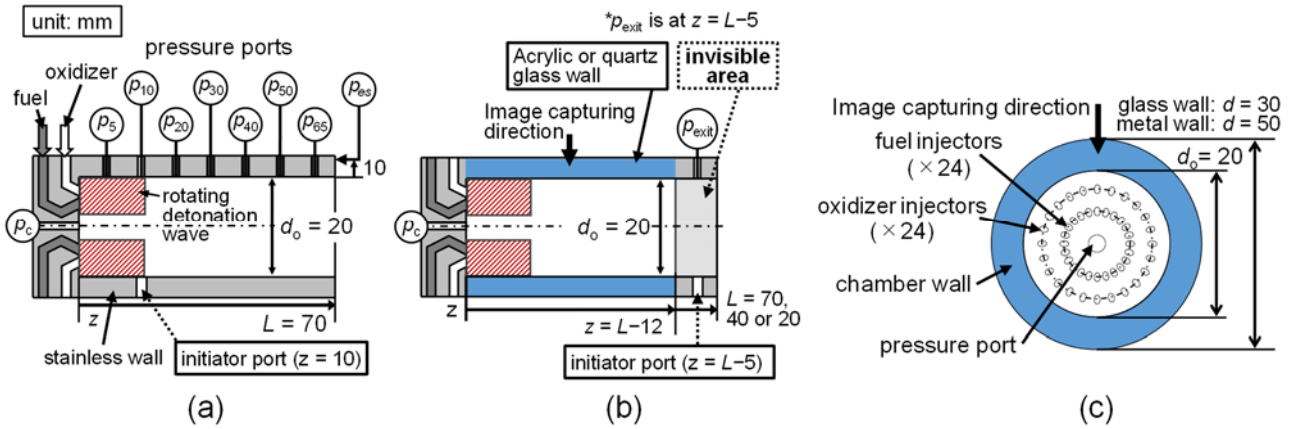

Fig. 1 Schematics of the cylindrical RDE: (a) the cylindrical RDE with a stainless wall used in pressure distribution measurement; (b) the optically accessible, cylindrical RDE with a glass wall; and detailed view of (c) the injector surface seen from the RDE exit.

M1: (58 mm + 10 mm) × 2.2 words/mm × 2 column + 40 words = 339 words

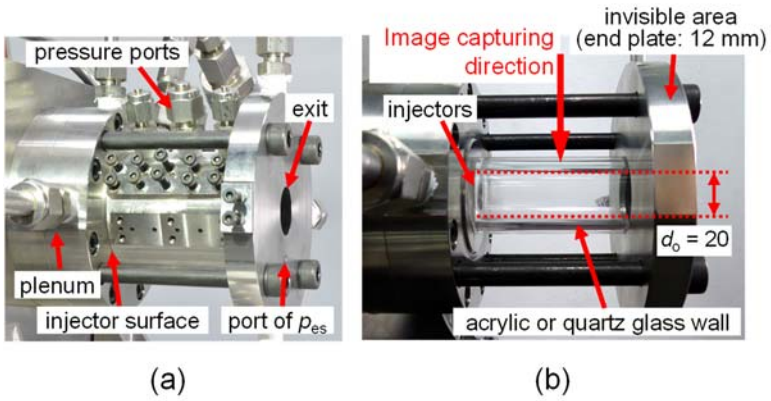

Fig. 2 Pictures of the two types cylindrical RDE: (a) the cylindrical RDE with the stainless wall; and (b) the optically accessible, cylindrical RDE with the glass wall.

M1: (55 mm + 10 mm) × 2.2 words/mm × 2 column + 26 words = 312 words

3. Results and discussion

The experimental conditions and a summary of the measurement results are presented in Table 1. We varied the propellant between Tests 1–6 (with C_2H_4–O_2) and Test 7 (with H_2–O_2). We also measured thrust in Tests 1–6, so specific impulse was obtained in these cases. Wall type was also different in each experiment. In Tests 1–3, we used the stainless combustor wall with seven pressure ports along the axial direction shown in Fig. 1a. In Tests 4–7, we used the glass wall in order to obtain self-luminescence images. In addition, PMMA and quartz were used in the optically accessible cylinder wall. The quartz wall was used in Test 4, and the PMMA wall in the other tests due to ready availability [21]. The quartz allows UV transmission and finer detail in the images, although this does not affect the discussion of the current paper.

The wave speed D was calculated from $D = \pi d/T$, where T is the period of the rotating wave, averaged using 10 cycles of rotation, and d is the diameter of the driving wave. Here, we assumed d = 15 mm. D was calculated using the axial pictures in Tests 1–6, because images were also captured from the axial direction in those cases. Although axial pictures were not taken and side pictures were used for the calculation in Test 7, the detonation speed was not affected by the distortion caused by the cylindrical window in the calculation method explained above. In all cases, the supersonic waves were observed in the combustor, and were sustained for the combustion duration (300 ms). This should mean the wave was

sustained and combined with the combustion, which is consistent with the definition of detonation combustion [2]. Therefore, the phenomenon in the combustor is regarded as detonation combustion.

Table 1. Experimental conditions and a summary of the measurement results.

Test	Propellant	Wall	L [mm]	$\dot{m}$ [g/s]	Φ [-]	p_b [kPa]	F [N]	I_{sp} [s]	D m/s
1*	C_2H_4-O_2	S/S**	70	27	1.3	6	59	226	1276
2*	C_2H_4-O_2	S/S**	70	36	1.8	11	88	246	1328
3	C_2H_4-O_2	S/S**	70	41	1.8	12	98	244	1336
4	C_2H_4-O_2	Quartz	70	26	1.3	45	46	183	1461
5	C_2H_4-O_2	PMMA	40	27	1.4	13	61	233	1294
6	C_2H_4-O_2	PMMA	20	27	1.3	13	56	213	1269
7	H_2-O_2	PMMA	70	22	1.5	100	-	-	1586

*The conditions and results of Tests 1 and 2 are cited from previous research [18]. **S/S = Stainless Steel

M1: (9 text lines + 2 lines) × 7.6 words/line × 2 columns + 23 words = 190 words

3.1 Heat release region and internal flow model of the cylindrical RDC

Figure 3 contains continuous images of self-luminescence captured by the high-speed camera at the side of the RDC. Figure 3a shows the images from Test 4 (C_2H_4-O_2 experiment), in which the images were captured at 2,000,000 frames/s (0.5 μs/frame), 127.5 μs duration, and with an exposure time of 0.5 μs. The black and white of the images are inverted in order to clarify the position of the strong luminance region. First, it may be observed that the strong self-luminescence (i.e., combustion) region spreads only near the bottom, from the bottom to 15–20 mm in the axial direction. This result confirms that the combustion of the RDC is completed near the injector surface. Figure 3b, which is the result of Test 7 (H_2–O_2 experiment), also supports this assumption. The images were captured at 1,000,000 frames/s for a duration of 256 μs with a short exposure time of 100 ns, which enabled us to obtain 10 samples in one cycle of a rotating wave. Self-luminescence captured in Fig. 3b is limited to chemical emission in the visible to near-IR, respectively, by the PMMA transmission spectrum and response of the camera intensifier. Reactions of H* and OH* (centered at 400–500 nm) and emission from high temperature water vapor (centered at 600–800 nm) [21, 22] are involved in the burned gas of H_2-O_2 combustion, and

luminance is uniform from near the injector. Therefore, we assume that combustion is completed near the injector even if the other propellant is used, and burned gas just flows to the chamber exit after the combustion region. This was also confirmed by the pressure measurement.

Other phenomena were observed in the continuous images. As indicated by the red dotted line in Fig. 3a, the strongest region of the luminance, which is assumed to be the detonation wavefront, looks like a forward-tilting wave. In the H_2-O_2 experiment, an interaction is observed between the shock wave extending to the exit and the burned gas. As shown in Fig. 3b, a "double-pole wave structure" appears in the chamber. This double-pole wave structure rotates around the center axis of the RDC while maintaining its structure, continuously generated from the bottom and moving to the exit. Hence, there is a shock wave in the chamber, but the burned gas flow is not affected so much, which means the flow structure is probably regarded as the steady phenomena. Although these transient phenomena involved with the detonation wave inside hollow RDCs are worth discussing, we focus on the steady phenomenon of internal flow and combustion phenomena.

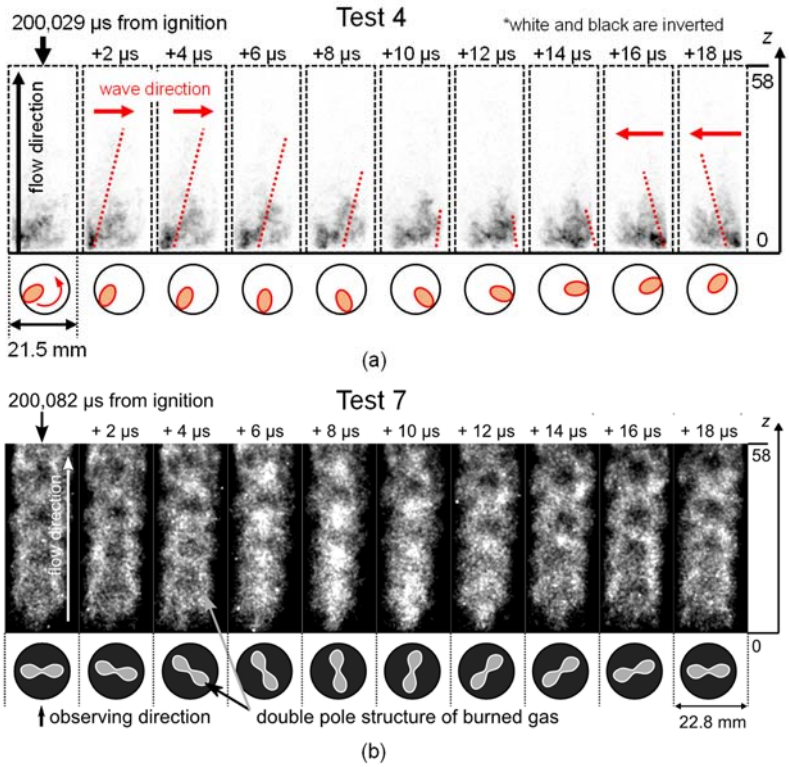

Fig. 3 Photographs of the self-luminescence taken from the radial direction in (a) Test 4 (C_2H_4–O_2), and (b) Test 7 (H_2–O_2) experiments (supplemental material: Movie S1 and S2).

M1: (104 mm + 10 mm) × 2.2 words/mm × 2 column + 26 words = 527 words

The most important point of the observations is that they strongly support the internal flow model assumption proposed in our previous paper [20]. Figure 4 shows the averaged luminance of Test 4 and pressure distribution measured in Tests 2 and 3. The slope of the pressure decreases along the axial direction and changes at z = 20 mm, a key phenomenon observed in our previous research. Here, luminescence observation confirms that the changing point of the slope is consistent with the strong luminescence region. Figure 5 shows the proposed scheme of the internal flow of a cylindrical RDC, based on pressure measurements in our previous study. In the model, following the intense heat release near the chamber bottom, burned gas is accelerated further by the effect of boundary layer growth and reaches sonic velocity at the chamber exit. This proposed model is called the "Rayleigh-flow boundary-layer-growth choking model."

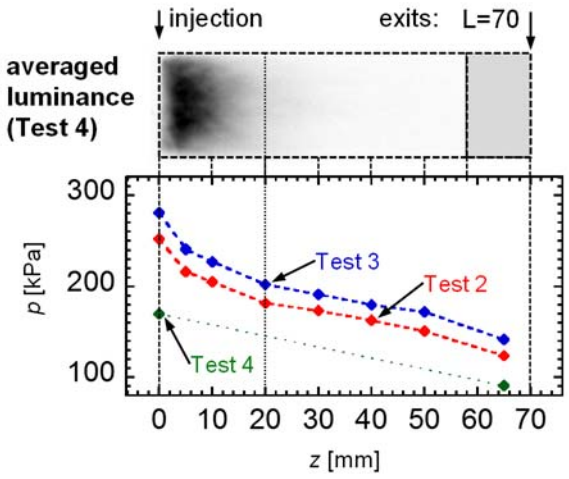

Fig. 4 Averaged luminance of Test 4 compared to the pressure distributions of Tests 2–4. Black and white in the image are inverted. Strong self-luminescence area spreads from the bottom to around 20 mm.

M1: (65 mm + 10 mm) × 2.2 words/mm + 33 words = 198 words

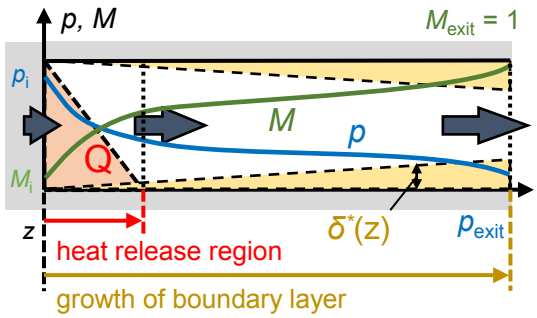

Fig. 5 Scheme of Rayleigh-flow and boundary-layer-growth choking model [20].

M1: (45 mm + 10 mm) × 2.2 words/mm + 8 words = 129 words

3.2 Performance of the cylindrical RDC with different chamber length conditions

Figures 3 and 4 and the measurement results of pressure distribution suggest that combustion is completed near the chamber bottom. As a result, we theorized that the chamber length of the RDC could be shortened without decreasing thrust performance. In order to confirm this, PMMA chamber walls shorter than 70 mm were made and combustion tests were conducted as Tests 5 and 6 in Table 1. Chamber length was 40 mm in Test 5 and 20 mm in Test 6. Other experimental conditions were the same as in Tests 1 and 4, except for the back-pressure condition of Test 4. We conducted experiments under these conditions and observed the detonation wave in shorter chambers, as depicted in Fig. 6. The velocities of the wave were almost the same in 3 cases (Tests 1, 5 and 6, which had the same test conditions except for chamber length). Here, $D = 1281 \pm 13$ m/s, as shown in Table 1. This suggests that chamber length does not affect the velocity of the detonation. Figure 7 compares the self-luminescence from the side in Tests 4–6. Note that the exit region of the chamber (to 12-mm from exit) is invisible due to the metal structure plate. It is clear that the combustion region in the shorter combustor conditions was distributed near the bottom, as in the 70-mm chamber length. The strong self-luminescence area finishes near the bottom, and self-luminescence is hardly observed beyond the chamber exit. This suggests that the chamber length of the RDC has little effect on the combustion phenomenon.

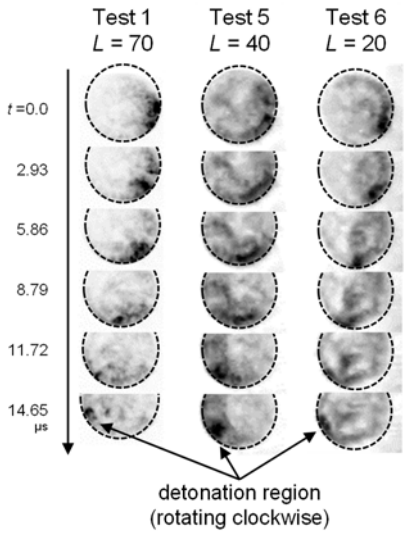

Fig. 6. Continuous axial photographs of single wave detonation observed in shorter chambers.

M1: (72 mm + 10 mm) × 2.2 words/mm + 12 words = 192 words

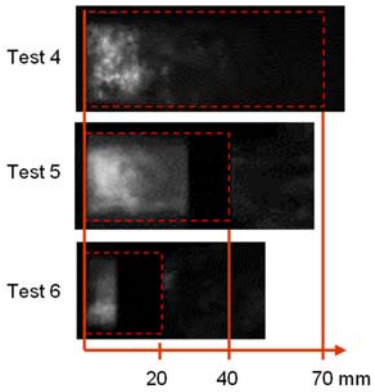

Fig. 7. Radial pictures of the cylindrical RDC with different chamber lengths.

M1: (52 mm + 10 mm) × 2.2 words/mm + 10 words = 146 words

Figure 8 shows the thrust performance of Tests 1, 5, and 6. Axial thrust in these test cases was within ±3 N, so measured thrust performance was also not affected by chamber length. Figure 9 compares the thrust performance of the shorter cylindrical combustor RDC with an annular 70-mm combustor. The solid line represents the theoretical specific impulse of RDCs ($I_{sp,\,theo}$) suggested in previous research based on the control surface theory [20], and the dashed line is the specific impulse calculated under the assumption that flow is expanded ideally ($I_{sp,\,ie}$). The specific impulse of the shorter chamber RDCs was 80–90% of the $I_{sp,ie}$. This suggests that combustion in the RDC is completed within the same length as the

chamber diameter (20 mm), and a cylindrical RDC with a shorter combustor has a thrust performance equal to the annular RDC.

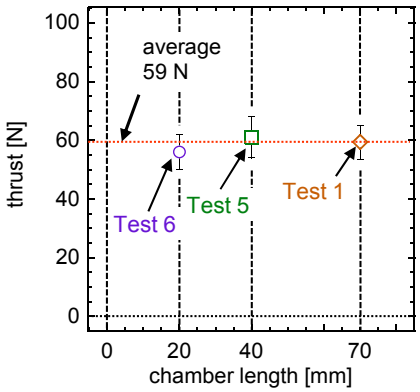

Fig. 8. Thrust of the cylindrical RDE in the different chamber length conditions. Experimental conditions are the same in Tests 1, 5, and 6.

M1: (54 mm + 10 mm) × 2.2 words/mm + 21 words = 162 words

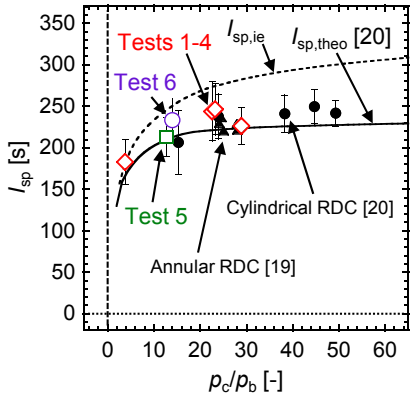

Fig. 9. Measured I_{sp} are plotted by the pressure ratio of p_c to p_b. Experimental I_{sp} of the cylindrical RDC measured in our previous research [20] (black circles) and an annular RDC measured by Kawasaki et al. [19] (black triangles) are also plotted.

M1: (54 mm + 10 mm) × 2.2 words/mm + 41 words = 181 words

Finally, we discuss the internal flow model of the shorter chamber RDC. Since Tests 5 and 6 were conducted using the glass wall chamber, we did not obtain the pressure distribution, and the pressure was measured only at the bottom and exit. Figure 10 shows pressure measured along the axial direction and calculated the pressure distribution based on the "Rayleigh-flow boundary-layer-growth choking model." The method for the modeled pressure distribution calculation was proposed in our previous study [20]. In the method, the governing equations in this model are as follows:

$$\frac{1}{\rho}\frac{\mathrm{d}\rho}{\mathrm{d}z}+\frac{1}{u}\frac{\mathrm{d}u}{\mathrm{d}z}+\frac{1}{A_{\mathrm{ef}}}\frac{\mathrm{d}A_{\mathrm{ef}}}{\mathrm{d}z}=0 \qquad (1)$$

$$u\frac{\mathrm{d}u}{\mathrm{d}z}+\frac{1}{\rho}\frac{\mathrm{d}p}{\mathrm{d}z}=0 \qquad (2)$$

$$\frac{\mathrm{d}}{\mathrm{d}z}\left[\rho u A_{\mathrm{ef}}\left(\frac{\gamma}{\gamma-1}\frac{p}{\rho}+\frac{u^2}{2}-\lambda Q\right)\right]=0 \qquad (3)$$

Here, u, p, ρ, A_{ef}, and λ ($0 \le \lambda \le 1$) represent axial velocity, pressure, density, effective cross-sectional area, and a reaction progress variable, respectively. These are variables of axial position z. Effective cross-sectional area $A_{\mathrm{ef}} = \pi/4(d_{\mathrm{o}}\text{-}2\delta^*)$ is the area of the chamber reduced by the boundary layer. δ^* is the displacement thickness of the boundary layer theory modeled as:

$$\delta^* = \frac{k}{R_z^{-1/5}}\, z \qquad (4)$$

where k is a constant coefficient involved in the extent of the boundary-layer-growth. The reaction progress variable λ represents the progress of chemical reaction or combustion: λ equals 0 before the onset of reaction, and $\lambda = 1$ indicates the completed reaction. We assume that combustion ends at a certain axial position z_{rc}, and then λ is defined as follows:

$$\lambda = -\frac{z}{z_{rc}^2}(z-2z_{rc}) \quad (z \le z_{\mathrm{rc}}) \qquad (5)$$

where λ is 0 at $z = 0$, and fixed at $\lambda = 1$ if z is larger than z_{rc}. k and z_{rc} are the fitting parameters of the Rayleigh-flow boundary-layer-growth choking model. The fitting parameter k is determined to satisfy the assumption of sonic velocity at the chamber exit.

In terms of parameters, z_{rc} is set as 20 mm as with the L = 70-mm case from self-luminescence observation, and k is 0.23 for Test 5 and 0.27 for Test 6 to satisfy $M = 1$ at the chamber exit. Other initial parameters are decided by experimental conditions. For example, the total released chemical energy per unit mass Q, which is calculated by the NASA-CEA constant pressure combustion mode, was 6300 kJ/kg for each case. Calculated results were close to measured pressure at the chamber exit. This result suggests that the "Rayleigh-flow boundary-layer-growth choking model" can be applied to RDCs with various conditions, such as different combustor geometries, mass flow rate, and equivalent ratios. Although the

interpretation of and decision method for coefficient *k* remains as future work, the proposed model and its conformity to the experimental results reveal that the time-averaged flow structure of the RDC is interpretable by the conventional governing equations of the compressible flow.

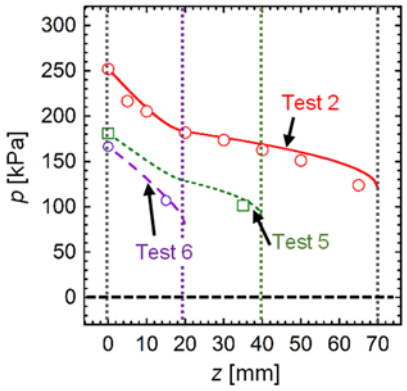

Fig. 10. Calculated pressure distributions of Tests 2, 5, and 6 based on Rayleigh-flow boundary-layer-growth choking model.

M1: (54 mm + 10 mm) × 2.2 words/mm + 14 words = 154 words

4. Conclusions

For the C_2H_4–O_2 and H_2–O_2 mixtures, the nozzle-less, cylindrical RDE was tested with an optically accessible chamber walls with different lengths. In the C_2H_4–O_2 tests, a strong self-luminescence area was observed near the chamber bottom. The region spread from the bottom to 20 mm, and when this is regarded as a heat release zone, it is consistent with the pressure distribution results. Tests were also conducted with the H_2–O_2 and axially uniform luminance was obtained. Since the luminance should derive from the emission of burned gas, the test with the other propellant also supported the assumption that combustion of RDCs is completed immediately. These experimental results are also consistent with the internal flow model proposed in our previous study (Rayleigh-flow boundary-layer-growth choking model), which was based on pressure distribution measurements.

Based on the self-luminescence observation results with a chamber length of 70 mm, we attempted to shorten the chamber length. Results revealed that the rotating detonation wave could be observed in a cylindrical RDC with shorter

chamber length (40 and 20 mm). Detonation wave velocity and thrust performance did not appear to be affected by the difference in chamber length. In other words, in an RDC in which the chamber had the same length as diameter, the combustion worked and the thrust performance was not altered compared to a cylindrical or annular RDC with a longer chamber length. Finally, we calculated the pressure distribution model of the RDC with various chamber lengths and results were consistent with the pressure measurements. This confirmed that the "Rayleigh-flow boundary-layer-growth choking model" can be applied to RDCs with various geometrical and supply conditions.

Acknowledgments

This study was financially supported by JSPS KAKENHI Grant Numbers JP19H05464, JP18KK0127, JP17H03480, JP17K18937, and by the Institute of Space and Astronautical Science of the Japan Aerospace Exploration Agency. Funding for high-speed imaging equipment used in this work was provided by AFOSR Award No. FA9550-16-1-0315 (Dr. Martin Schmidt, Program Officer). The authors would like to acknowledge the US Department of Energy for the part-time faculty appointment of Prof. Paniagua to the Faculty Research Participation Program at the National Energy Technology Laboratory and the support of James Braun in part by an appointment to the National Energy Technology Laboratory Research Participation Program, sponsored by the U.S. Department of Energy and administered by the Oak Ridge Institute for Science and Education.

References

[1] W. Fickett, W. C. Davis, Detonation: Theory and Experiment, Dover Publications, New York, 2000.

[2] J. H. S. Lee, The Detonation Phenomenon, Cambridge University Press, Cambridge, 2008.

[3] P. Wolanski, Detonative Propulsion, Proc. Combust. Inst. 34 (1) (2013) 125-158.

[4] K. Kailasanath, Review of Propulsive Applications of Detonation Waves, AIAA J. 38 (9) (2000)

1698–1708.

[5] F. K. Lu, E. M. Braun, Rotating Detonation Wave Propulsion: Experimental Challenges, Modeling, and Engine Concepts, J. Propul. Power 30 (5) (2014) 1125-1142.

[6] G. D. Roy, S. M. Frolov, A. A. Borisov, D. W. Netzer, Pulse Detonation Propulsion: Challenges, Current Status, and Future Perspective, Prog. Energy Combust. Sci. 30 (6) (2004) 545-672.

[7] M. Yamaguchi, K. Matsuoka, A. Kawasaki, J. Kasahara, H. Watanabe, A. Matsuo, Supersonic combustion induced by reflective shuttling shock wave in fan-shaped two-dimensional combustor, Proc. Combust. Inst. 37 (3) (2019) 3741-3747

[8] B. A. Rankin, D. R. Richardson, A. W. Caswell, A. G. Naples, J. L. Hoke, F. R. Schauer, Chemiluminescence imaging of an optically accessible non-premixed rotating detonation engine, Combust. Flame 176 (2017) 12-22.

[9] B. A. Rankin, J. R. Codoni, K. Y. Cho, J. L. Hoke, F. R. Schauer, Investigation of the structure of detonation waves in a non-premixed hydrogen–air rotating detonation engine using mid-infrared imaging, Proc. Combust. Inst. 37 (3) (2019) 3479-3486.

[10] F. Chacon, M. Gamba, Study of Parasitic Combustion in an Optically Accessible Continuous Wave Rotating Detonation Engine, AIAA Scitech 2019 Forum, San Diego, 2019, 2019-0473.

[11] F. Chacon, M. Gamba, OH PLIF Visualization of an Optically Accessible Rotating Detonation Combustor, AIAA Propul. Energy Forum 2019, Indianapolis, 2019.

[12] M. D. Bohon, R. Bluemner, C. O. Paschereit, E. J. Gutmark, High-speed imaging of wave modes in an RDC, Exp. Therm. Fluid Sci. 102 (2019) 28-37.

[13] V. Athmanathan, J. Braun, Z. Ayers, J. Fisher, C. A. Fugger, S. Roy, G. Paniagua, T. R. Meyer,

Detonation structure evolution in an optically-accessible non-premixed H_2-Air RDC using MHz rate imaging**,** AIAA Scitech 2020 Forum, Orlando, 2020, 2020-1178.

[14] C. Knowlen, E. A. Wheeler, M. Kurosaka. Thrusting Pressure and Supersonic Exhaust Velocity in a Rotating Detonation Engine, 2018 AIAA Aerospace Sci. Meeting, Kissimmee, 2018, 2018-1884.

[15] K. Goto, J. Nishimura, A. Kawasaki, K. Matsuoka, J. Kasahara, A. Matsuo, I. Funaki, D. Nakata, M. Uchiumi, K. Higashino, Propulsive Performance and Heating Environment of Rotating Detonation Engine with Various Nozzles, J. Propul. Power, 35 (1) (2019) 213-223.

[16] X. M. Tang, J. P. Wang, Y. T. Shao, Three-Dimensional Numerical Investigations of the Rotating Detonation Engine with a Hollow Combustor, Combust. Flame 162 (4) (2015) 997-1008.

[17] W. Lin, J. Zhou, S. Liu, Z. Lin, An Experimental Study on CH4/O2 Continuously Rotating Detonation Wave in a Hollow Combustion Chamber, Exp. Therm. Fluid Sci. 62 (2015) 122-130.

[18] V. Anand, A. C. St. George, E. J. Gutmark, Hollow Rotating Detonation Combustor, 54th AIAA Aerospace Sci. Meeting, San Diego, 2016, 2016-0124.

[19] A. Kawasaki, T. Inakawa, J. Kasahara, K. Goto, K. Matsuoka, A. Matsuo, I. Funaki, Critical Condition of Inner Cylinder Radius for Sustaining Rotating Detonation Waves in Rotating Detonation Engine Thruster, Proc. Combust. Inst. 37 (3) (2019) 3461-3469.

[20] R. Yokoo, K. Goto, J. Kim, A. Kawasaki, K. Matsuoka, J. Kasahara, A. Matsuo, I. Funaki, Propulsion Performance of Cylindrical Rotating Detonation Engine, AIAA J. (2019) Published Online.

[21] R. W. Schefer, W. D. Kulatilaka, B. D. Patterson, T. B. Settersten, Visible emission of hydrogen flames, Combust. Flame 156 (6) (2009) 1234-1241.

[22] A. G. Gaydon, The Spectroscopy of Flames, 2nd ed., Chapman and Hall, London, 1974.

Table and figure captions

Table 1	Experimental conditions and a summary of the measurement results. *The conditions and results of Tests 1 and 2 are cited from previous research [18].
Fig. 1	Schematics of the cylindrical RDE: (a) the cylindrical RDE with a stainless wall used in pressure distribution measurement; (b) the optically accessible, cylindrical RDE with a glass wall; and detailed view of (c) the injector surface seen from the RDE exit.
Fig. 2	Pictures of the two types cylindrical RDE: (a) the cylindrical RDE with a metal wall; and (b) the optically accessible, cylindrical RDE with a glass wall.
Fig. 3	Photographs of the self-luminescence taken from the radial direction in (a) Test 4 (C_2H_4–O_2) and (b) Test 7 (H_2–O_2) experiments (supplemental material: Movie S1 and S2).
Fig. 4	Averaged luminance of Test 4 compared to the pressure distributions of Tests 2–4. Black and white in the images are inverted. Strong self-luminescence area spreads from the bottom to around 20mm.
Fig. 5	Scheme of Rayleigh-flow and boundary-layer-growth choking model [18].
Fig. 6	Continuous axial photographs of single wave detonation observed in shorter chambers.
Fig. 7	Radial pictures of the cylindrical RDC with different chamber lengths.
Fig. 8	Thrust of the cylindrical RDE in the different chamber length conditions. Experimental conditions are the same in Tests 1, 5, and 6.
Fig. 9	Measured I_{sp} are plotted by the pressure ratio of p_c to p_b. Experimental I_{sp} of the cylindrical RDC measured in our previous research [18] (black circles) and an annular RDC measured by Kawasaki et al. [17] (black triangles) are also plotted.
Fig. 10	Calculated pressure distributions of Tests 2, 5, and 6 based on Rayleigh-flow boundary-layer-growth choking model.

Supplemental Material (Movie captions)

Movie S1	Photograph taken from the side of the RDE in Test 4 (C_2H_4–O_2 case). Black and white in the images are inverted.
Movie S2	Photograph taken from side of the RDE in Test 7 (H_2–O_2 case).